ELECTROCHEMISTRY RESEARCH LABORATORY

DEPARTMENT OF CHEMISTRY

JOHN SCHOFF MILLIS SCIENCE CENTER

CASE WESTERN RESERVE UNIVERSITY

CLEVELAND, OHIO 44106

Semi-Annual Status Report No. 8

1 October 1975 to 31 March 1976

CATALYSTS FOR ELECTROCHEMICAL GENERATION OF OXYGEN

Report Prepared by: W. E. O'Grady

Project Director: Ernest Yeager

NATIONAL AERONAUTICS AND SPACE ADMINISTRATION

NASA-Ames Grant No. NGR 36-027-050

ELECTROCHEMISTRY RESEARCH LABORATORY

Department of Chemistry
John Schoff Millis Science Center
CASE WESTERN RESERVE UNIVERSITY
Cleveland, Ohio 44106

Semi-Annual Status Report No. 8

1 October 1975 to 31 March 1976

CATALYSTS FOR ELECTROCHEMICAL GENERATION OF OXYGEN

Report Prepared by: W. E. O'Grady

Project Director: Ernest Yeager

NATIONAL AERONAUTICS AND SPACE ADMINISTRATION
NASA-Ames Grant No. NGR 36-027-050

TABLE OF CONTENTS

LIST OF FIGURES

Section III-2

Chemistry Department
Case Western Reserve University
Cleveland, Ohio 44106

CATALYSTS FOR THE ELECTROCHEMICAL GENERATION OF OXYGEN

Semi-Annual Status Report for 1 October 1976 to 31 March 1976

Sponsor: NASA-Ames

Grant No.: NGR 36-027-050

I. PRIMARY OBJECTIVES

1. To find new, more effective catalysts for the electrolytic evolution of oxygen and to understand the mechanism and kinetics for the electrocatalysis in relation to the surface electronic and lattice properties of the catalyst, as well as developing an understanding of the structural features of the electrocatalysts which are critical to high electrochemical activity for the anodic generation of O_2.

2. To evaluate the kinetics and mechanism of anodic generation of O_2 under well defined conditions in relation to the properties of the electrode surface.

II. SPECIFIC OBJECTIVES FOR THIS REPORTING PERIOD

1. Initial experiments with the LEED-Auger-thin-layer electrochemical system on Pt (111). Paper presented at the May, 1976 meeting of the Electrochemical Society in Washington, D. C.

2. Paper on Oxygen Electrocatalysts for Life Support Systems to be presented at the Sixth Annual Intersociety Conference on Environmental Systems.

III. SUMMARY OF THE WORK

1. LEED-Auger studies of electrode surfaces

To establish the relationship between the electrocatalytic and corrosion processes occurring at the electrochemical interface and the atomic structure of the metal surface, a new level of experimentation is required. To date in single crystal studies there has been no

assurance that the micro-structure of the surface is that corresponding to the macro-orientation of the sample or that the surface composition reflects that of the bulk. Furthermore, the role of impurities on the metal electrode surface has not been clearly resolved. The difficulties which have recently become apparent in cleaning metal surfaces in gas phase studies have strong implications for electrochemists.

The methods of electron physics, low energy electron diffraction (LEED), Auger electron spectroscopy (AES) and x-ray photoelectron spectroscopy (XPS) are powerful tools for characterizing surfaces. With few exceptions (1,2), however, electrochemists have been reluctant to use non in situ techniques to obtain such information because of the changes anticipated in transferring the electrode between the electrolyte and high vacuum environments.

In order to minimize these changes and to utilize these powerful techniques of electron physics a system has been assembled which combines LEED and AES with thin-layer electrochemical methods and low temperature vacuum sublimation and transfer techniques. The system consists of two separate ultra high vacuum chambers as shown in Figure 1. One chamber contains the LEED-Auger electron spectrometer while the second chamber houses the electrochemical thin-layer cell and other sample preparation methods. The two chambers are completely isolated by an all metal bakeable valve which allows the sample to be transferred between the two chambers.

The LEED-AES system is a standard Varian system utilizing retarding field analysis of the electron energies. The sample holder is a

modified Varian manipulater which allows the sample to be removed for transfer to the second vacuum chamber while retaining the features of being able to heat the sample to 1200 K and cooled to 100 K.

In the second chamber is a liquid nitrogen cooled manipulator which allows the sample to be removed for transfer and also positions the sample in the thin layer cell. The transfer of the sample from the LEED-AES chamber to the electrochemical chamber is accomplished by a UHV transfer mechanism with a spring clip holder on the end for holding the sample during the transfer.

Two primary experiments are underway with this system. The first involves cleaning and LEED-Auger characterization of the metal surface and then studying electrochemistry on this surface. The second involves returning the single crystal electrode to the LEED-Auger spectrometer after electrochemical treatment and characterization. In the first a single crystal of platinum has been oriented in the (111) direction and cleaned to the limits of detection of AES (0.01% mono-layer). The main impurities found on the platinum were sulfur and carbon. The impurities are removed by argon ion sputtering with subsequent high temperature annealling. The Auger spectra of the contaminated and cleaned surface are shown in Figure 2. After the surface is annealed the standard hexagonal LEED pattern for Pt (111) is obtained.

The cleaned and annealed sample is then transferred to the second chamber under UHV. This chamber is back filled with purified argon and the sample is placed in the thin-layer electrochemical cell. The potential region between 0 and 0.4 V (NHE) is scanned and the behavior of the cyclic voltammogram on the clean Pt (111) surface is shown in Figure 3.

This voltammogram was taken in 10^{-3} M $HClO_4$. The shape of the curve is not that normally found for $HClO_4$ (3). It appears to be contaminated with chloride ion. Also, the combined reference-counter electrode may be shifting in potential causing the positions of the peaks to be displaced.

REFERENCES

(1) A. T. Hubbard, R. M. Ishikawa and J. A. Schoeffel, in Proc. Symp. Electrocatalysis, Ed., M. Breiter, pg. 258, Electrochemical Society, Princeton, N. J. 1974.

(2) J. A. Joebstl, First Chemical Congress of the North American Continent, Mexico City, Mexico, Abstract PHSC 18.

(3) Semi-Annual Status Report #7, 1 April 1975 to 30 September 1975, Catalysts for Electrochemical Generation of Oxygen, W. E. O'Grady, J. Huang and E. Yeager, NASA-Ames Grant No. NGR 36-027-050.

2. Oxygen Electrocatalysts for Life Support Systems (by W. E. O'Grady, C. Iwakura and E. Yeager)

Presented at the Intersociety Conference on Environmental Systems, SanDiego, California, July 12-15, 1976. (See Appendix)

IV. PROJECTED WORK

Research during the upcoming six months will concentrate on the electrochemical characterization of the several crystal faces of platinum, using LEED-Auger Electrochemical System.

V. PROJECT PERSONNEL

Patrick Hagans, Graduate Student

Marino Woo, Graduate Student

William O'Grady, Senior Research Associate

Ernest Yeager, Professor of Chemistry, Project Director

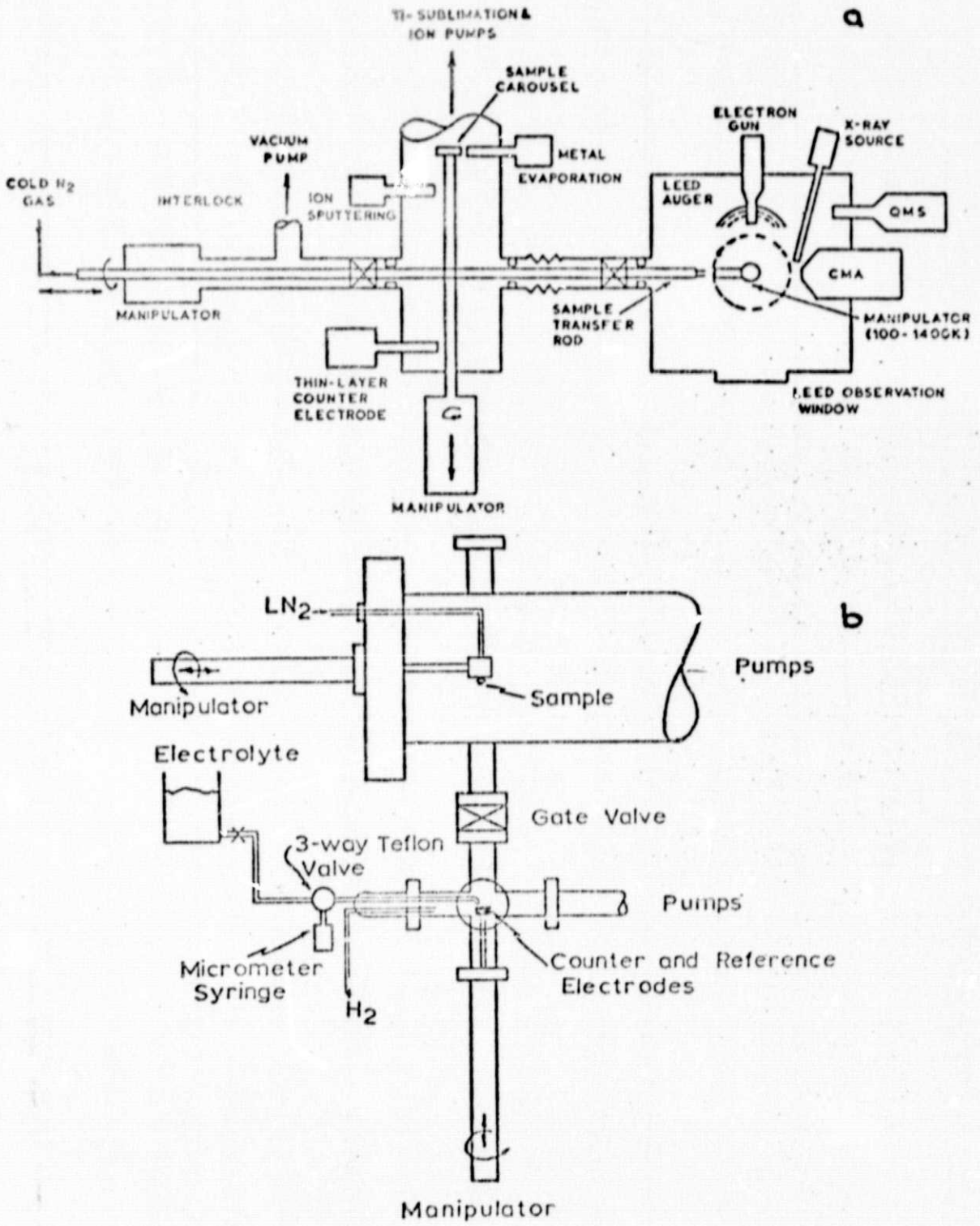

Figure 1. Schematic drawings of (a) the LEED-Auger-thin layer electrochemical system and (b) details of the solution injection and thin-layer cell system.

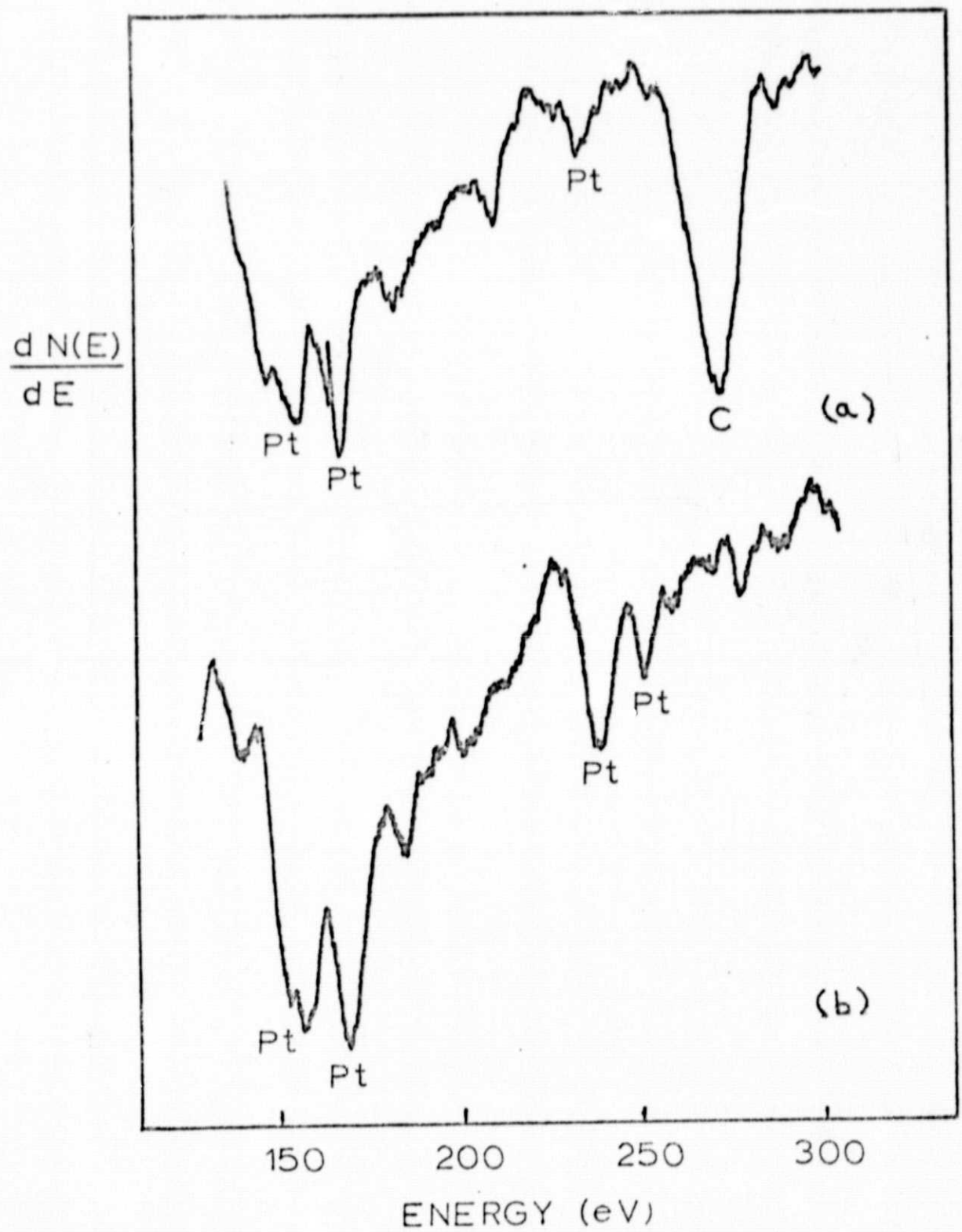

Figure 2. Auger Spectra of Pt (111) (a) contaminated (b) after aron-ion sputter cleaning.

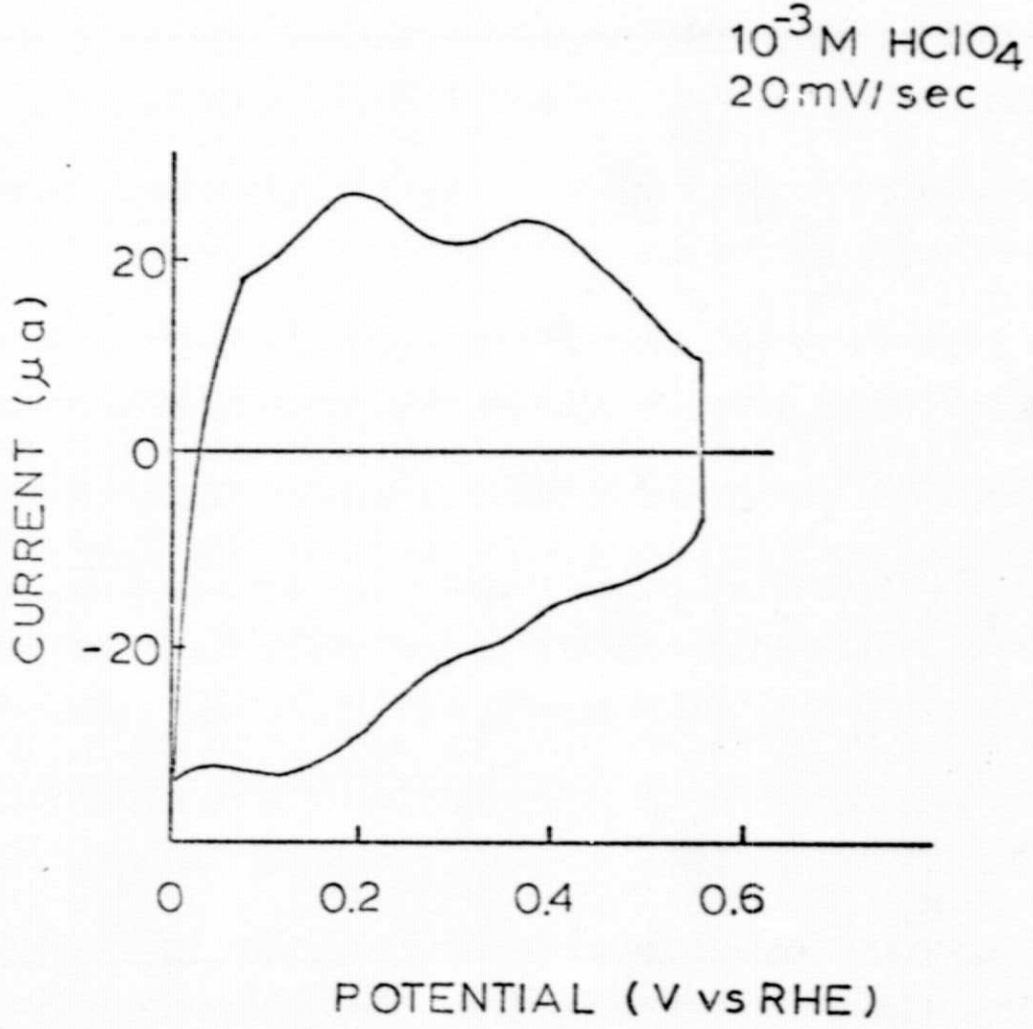

Figure 3. Cyclic Voltammogram of Pt (111). First sweep in 10^{-3} M $HClO_4$ sweep rate 20 mV/sec.

APPENDIX

OXYGEN ELECTROCATALYSTS FOR LIFE SUPPORT SYSTEMS

by

W. E. O'Grady, C. Iwakura*and E. Yeager

The Electrochemistry Laboratory
Chemistry Department
Case Western Reserve University
Cleveland, Ohio 44106

Abstract

The irreversibility of the oxygen electrode increases by 30 to 60% the energy required for water electrolysis over the thermodynamic value in life support systems involving conventional water electrolysis cells. To minimize this voltage loss, high area electrocatalysts such as platinum metal are often used for the O_2 anode but even so, the losses are still very substantial. In an attempt to find more effective electrocatalysts for this application, a number of defect metal oxides have been examined.

I. INTRODUCTORY BACKGROUND

In water electrolyzers, ohmic losses and electrode polarization result in substantial loss of efficiency in the use of electrical energy to produce O_2 and H_2. Even in modern water electrolyzers operating below 200°C, the cell terminal voltages at reasonable current densities ($>100 mA/cm^2$) usually exceed the reversible (thermodynamic) values[a] by 25 to 50%. To achieve

---

*Present address: Department of Applied Chemistry, Faculty of Engineering, Osaka University, Suita, Osaka, Japan.

[a]The reversible cell voltage for water electrolysis depends on the electrolyte, pressure and temperature. For cells for which the molefraction of water is >0.8 and the O_2 and H_2 pressures are each $\sim$1 atm, the reversible voltage is 1.23V at 25°C and 1.17V at 100°C. For a pressurized electrolyzer with 50% (by weight) KOH and O_2 and H_2 pressures of 15 atm, the reversible voltage is 1.03V at 264°C (2).

acceptable operating efficiencies, it is necessary to restrict the current densities to relatively low values with corresponding increments in the weight, volume and cost of the electrolyzer.

Some voltage losses, however, are usually desirable within water electrolyzers. The entropy change ΔS for the production of H_2 and O_2 from water is negative and hence the electrolysis of water under reversible conditions is endothermic. The ohmic and electrode polarization losses can provide this $T\Delta S$ heat as well as the additional heat to offset heat losses to the surroundings with cells operating above ambient temperatures.

For a water electrolysis cell operating at a cell terminal voltage of E, the heat generated within the cell per mole of O_2 produced is

$$Q = 4F(E - E_{rev}) + T\Delta S = 4FE + \Delta H \qquad (1)$$

where F is the Faraday, E_{rev} is the reversible cell potential and ΔH and ΔS are the enthalpy and entropy changes for the reaction

$$H_2O(\ell) \longrightarrow 2H_2 + O_2 \qquad (2)$$

The thermoneutral potential E_{TN} is defined as the value of E in equation 1 such that Q = 0. Therefore,

$$E_{TN} = -\Delta H/(4F) \qquad (3)$$

The heat loss from the cell can be reduced to a value low compared to ΔH, and therefore, the thermoneutral potential represents a reasonable target voltage in reducing various

types of voltage losses. For water electrolyses cells with pure liquid water at 25°C fed into the cells and H_2 and O_2 exiting at this same temperature after passing through suitable heat exchangers, the thermoneutral potential is 1.48V; for 100°C, the value is 1.45V.

While several of the advanced electrolyzers represented in Figure 1 have cell voltages close to the thermoneutral potential at low current densities, all exceed this value by appreciable amounts at the higher current densities which are attractive in most instances for compact electrolyzers. Thus, even considering the thermoneutral potential, it is attractive to find ways for further reducing voltage losses at high current densities.

II. PRESENT STATUS OF O_2 ELECTROCATALYSTS FOR WATER ELECTROLYZERS

In most water electrolyzers, polarization at the O_2 anode is the largest source of voltage loss. This polarization arises because of the irreversibility of the electrochemical reactions involved in the formation of O_2 from oxygen of water. Three approaches are available for reducing the electrode polarization at high current densities: 1) electrode surfaces with high intrinsic electrocatalytic activity for the O_2 generation reaction; 2) ultra high area electrocatalysts; and 3) operation at elevated temperatures. All three approaches have been applied. Nickel has been most extensively used as the O_2 anode surface in water electrolyzers using concentrated NaOH or KOH as the electrolyte. Under operating conditions a high area oxide film forms on the anode. The overpotentials at reasonable

current densities[b], however, are still high (e.g., 0.4V at 100 mA/cm^2 at 80°C (2)) unless the cells are operated at temperatures above 175°C. This requires pressurization and furthermore can lead to electrode stability problems.

For life support systems for space, high area platinum is presently used for the anode electrocatalyst. This surface has relatively high overpotential at moderate current densities even at normal temperatures (0.3V at 100 mA/cm^2 at 22°C - See Figure 2) but the overpotential is still higher than desired and platinum cost can be a problem for some water electrolyzer applications.

III. CRITERIA FOR O_2 CATALYSTS FOR WATER ELECTROLYZERS

The present research represents an effort to find O_2 anode catalysts superior to high area Pt. In evaluating catalysts four criteria must be considered:

1. Electrocatalytic Activity

Over a significant range of current densities most electrode processes, including the oxygen electrode follow the Tafel equation; i.e.

$$\eta = E - E_{rev} = B(\log i - \log i_o) \qquad (4)$$

where η is the overpotential, i is the apparent current density and B is a temperature dependent constant. The exchange current density i_o is usually used as a criteria of catalyst activity.

---

[b]All current densities are per unit apparent area unless otherwise indicated.

Since i is many orders of magnitude greater than i_o for all presently known O_2 electrocatalysts, it is also important that the slope constant B be as low as possible. For the high area Pt electrode represented in Figure 2, i_o is $\sim 2 \times 10^{-5}$ A/cm^2 while the Tafel slope B is $\sim$ 0.10V/decade.

2. Electronic Conductivity

It is necessary that the catalyst phase have reasonable electronic conductivity. With Pt electrodes, the catalyst phase is an oxide layer of several monolayers formed in situ. Present indications (3) are that electron transfer through this film occurs by tunnelling and is sufficiently slow to contribute substantially to the oxygen overpotential. With catalyst layers or particles of the order of 10^{-4}cm, the resistivity must be less than 10^3 ohm-cm.

3. Stability

This requires that the catalyst have very low solubility in the electrolyte, not undergo undesirable changes in valency state and not be very susceptible to trace poisons. High area catalysts are usually involved and these must not undergo sintering or Oswald ripening under the cell operating conditions.

4. Catalyst Cost

For most life support applications, the catalyst cost is likely to be a secondary consideration provided the catalyst cost does not exceed some reasonable value such as $1.00 per watt of power consumed. Even heavily loaded Pt electrodes are still well below this figure at reasonable current densities.

The situation is quite different for commercial water electrolyzers, for which catalyst costs in excess of $0.05 per watt are probably prohibitive.

The present knowledge of O_2 anodic electrocatalysis does not provide a strong basis for deciding which catalyst systems are best candidates for screening. Despite extensive studies of O_2 generation mostly on Pt, the reaction mechanism is still not well established. The O_2 anode is sufficiently irreversible that the back reaction is negligible even at low current densities. This has made it difficult to establish the mechanism for O_2 generation since only steps up to the rate-controlling one (usually the first electron transfer) can be examined. Measurements near the reversible potentials are impractical because of competing reactions intrinsic to the electrode surface and impurity currents. The extensive kinetic studies of O_2 reduction have not proved very helpful in understanding the anodic process because the reduction occurs at appreciable rates only at potentials very cathodic (by at least 0.5V) to those for O_2 generation. The surface conditions prevailing at these potentials are not the same, and, therefore, the kinetics and even the pathways can be expected to be different for the anodic and cathodic processes. To complicate the situation further, a large number of pathways are possible for O_2 generation and reduction.

IV. O_2 ELECTROCATALYSIS ON DEFECT METAL OXIDES

Transition metal oxides head the list of promising oxygen anode catalysts since the transition metal ions are expected to

interact with various intermediates in the O_2 anodic reaction and many have good electronic conductivity and good stability particularly in alkaline electrolytes. Rather than forming these oxides anodically in situ on the metal electrodes, the oxides have been formed ex situ in the present study by thermal decomposition of transition metal salts or a suitable substrate such as titanium. Oxides so formed have a highly defective structure and high internal pore surface area. Several such oxides have been found to be attractive.

Potential current curves are shown in Figure 3 for several transition metal oxides on a Ti support electrode. The curves at lower current densities ($< 10^{-5}$ A/cm^2) are strongly influenced by intrinsic changes in valency state of the oxide even though the data were acquired with decreasing current with three minutes at each data point. Since the current densities are apparent values, area differences may have influenced the relative positions of the curves.

Kinetic studies of O_2 generation have usually indicated the first electron transfer step to be rate controlling. If the stability of an adsorbed intermediate (e.g., the OH radical) formed in this step can be increased, then the rate control may shift to a later step such as the second electron transfer.[c] With O_2 generation on Pt, the situation appears to correspond

---

[c] A specific mechanism is proposed later in the discussion of the results for RuO_x.

to Curve I in Figure 4. With defect oxides such as ruthenium and iridium oxides, the situation appears to correspond to Curve II. The principal evidence for such is the Tafel slope of 0.04 to 0.05V/decade exhibited by these oxides in alkaline solutions, as compared with 0.1 to 0.24V/decade found with Pt.

The behavior of the corresponding pure metals as O_2 anodes is distinctly different from that of the defect metal oxides in Figure 3 even though the metals are oxide coated at the potentials where O_2 generation occurs. Ruthenium metal is not stable as an O_2 anode in 4 M KOH; active dissolution begins at $\sim$1.3V vs. RHE.

V. RUTHENIUM OXIDE AS AN O_2 ANODE CATALYST

Of special interest is ruthenium oxide, produced by the thermal decomposition of ruthenium salts on a titanium support. This catalyst combines high electronic conductivity with low oxygen overpotential at high current densities even at room temperature (4). Further it has good stability in high area form in caustic solutions. The exchange current density is comparable to that of platinum but the Tafel slope is considerably lower (0.04 V per decade of current density) than with platinum (Figure 2), resulting in lower overpotentials at practical current densities.

A. Experimental

Oxygen generation on defective RuO_x has been studied in some detail (4). The preparation of this oxide involves the thermal decomposition of $RuCl_3$ on an appropriate metal substrate in a manner similar to that described in the patent literature (5)

for the dimensionally stable anodes (DSA) used in the chlor-alkali industry. Titanium metal was used for the substrate (99.95% Ti supplied by Research Organic-Inorganic). After polishing the Ti with emery and thorough cleaning, including degreasing by refluxing in isoproponal vapor, the surface was coated with a solution of reagent grade $RuCl_3$ (Fisher) in 20% HCl.

In order to vary the cataiyst loading on the electrode surface while maintaining an essentially constant preparative procedure, varying amounts of the original solution (0.1M Ru) were diluted to the same volume and this solution then applied to the substrate in six repetitive coatings or alternatively the number of coatings varied. After each coating, the solution was dried at a moderate temperature (110°C in a drying oven for 5 min.) and then placed in a preheated furnace at 350°C for 10 min. After the final coating, the temperature of the furnace was raised to 450°C for 1 hour. The catalyst loadings examined in the present work ranged from 10^{-9} to 10^{-5} moles of Ru per cm^2. Other substrate materials have also been examined; namely gold, tantalum, platinum and nickel. The substrate has no direct effect on the electrocatalytic activity, expressed per unit true area of the RuO_x for catalyst loadings of 10^{-7} to 10^{-5} moles of RuO_x per cm^2 of geometric area. Titanium is preferred to Au, Ta, Pt or Ni as a substrate because the RuO_x forms a more uniform and adherent layer on Ti.

The majority of the measurements have been carried out

with 4M KOH prepared from reagent grade KOH (Baker, 0.2% carbonate) and triply distilled water (second stage from alkaline permanganate). For the pH dependence studies, different ratios of 1M KOH and 0.5M K_2SO_4 were used. For the rotating disk experiments, the solutions were pre-electrolyzed in a separate Teflon cell between bright nickel electrodes (7 cm^2 each) at a current density of 1 ma/cm^2 for a minimum of 24 hr with agitation obtained using purified helium gas (6).

O_2 reduction as well as generation were studied on the RuO_x/Ti electrodes using the rotating disk electrode technique. The rotating disk experiments were carried out in an all Teflon cell (7) consisting of a main compartment containing the working electrode and two separate compartments for the reference and counter electrodes, both of which were Pd-H in the form of Pd diaphragms supplied with H_2 from the back side. The reference compartment was connected to the main working electrode compartment by a Teflon Luggin capillary positioned at 4 mm from the rotating disk electrode surface on the axis of rotation. The electrolyte in the main compartment was usually saturated with purified O_2 gas (6).

A Wenking potentiostat, a linear sweep generator and Houston x-y recorder were used to carry out the electrochemical measurements. The essentially steady state polarization data were obtained with very slow voltage sweeps (1 mV/sec) and in some instances also with point by point measurements (e.g., 3 min per point) as a check. The IR drop corrections, needed at

higher current densities, were determined using the current interrupter technique with a high pressure hydrogen, mercury-wetted relay to interrupt the current.

B. Results

1. Electrochemical area

The Zn^{2+} ion adsorption technique, developed by Kozawa (6) has been used to obtain an estimate of the ratio of true-to-apparent area for the RuO_x on Ti electrodes. This method is preferred to the usual BET measurements since pores that may not necessarily be electrochemically accessible may contribute to the BET areas.

The Zn^{2+} adsorption method is based on the concept that the Zn^{2+} will ion exchange with H^+ bound to surface $O^=$, releasing H^+ into the solution. The assumption is made that the surface coverage with Zn^{2+} is near or at saturation and that the area per Zn^{2+} has a specific value. Kozawa has demonstrated the validity of the method for battery oxides such as MnO_2 with the Zn^{2+} adsorption measured by the decrease in Zn^{2+} concentration in a $ZnCl_2$-NH_4Cl solution and the area taken to be 17 $\mathring{A}^2$ per adsorbed Zn^{2+}.

In the present study, the Zn^{2+} ion adsorption was measured on the RuO_x coated flat titanium electrodes by placing them in a 0.5$\underline{M}$ NH_4Cl solution containing 0.005$\underline{M}$ Zn^{+2} at a pH of 7.25. Overnight was allowed for equilibrium and an alloquote of the solution then titrated with EDTA using Erichrome Black T as the indicator.

Using an area of 20 $\mathring{A}/Zn^{2+}$, this method yields a ratio of true-to-apparent surface area of typically 60 - 80 for a catalyst loading of 1×10^{-5} moles Ru/cm^2 of geometric area. Studies of the adsorption isotherms for Zn^{2+} on dispersed RuO_x (without potential control) indicate that the Zn^{2+} adsorption is not at saturation under the above conditions (9). Therefore, the true-to-apparent surface area ratio measured by the Zn^{2+} adsorption method can only be viewed as lower limiting values.

Using krypton BET, Kuhn and Mortimer (10) found a ratio of 240 for their RuO_x on Ti electrodes. While the technique used to prepare their electrodes is similar to that in the present work, their catalyst loading is not specified. Since more concentrated Ru solutions (0.4M) were used by Kuhn and Mortimer for coating their electrodes, the thickness of the RuO_x coatings on their electrodes may well have been several fold greater.

2. Voltammetry curves for RuO_x

Typical slow sweep voltammetry curves are shown in Figure 5 in N_2-saturated alkaline and acid solutions. Some minor features of the curves in the voltage range 0.6 - 1.0V are associated with the O_2/H_2O_2 couple. The peak at ~1.3V in the alkaline solution is only slightly irreversible at the sweep rate of 50 mV/sec. At slower sweep rates (e.g., 10 mV/sec) this peak is essentially reversible with the anodic and cathodic peak potentials coinciding.

This peak, however, has not been observed for RuO_x on nickel or platinum or for the uncoated titanium. Thus the peak

appears to involve the interaction of the RuO_x with the Ti substrate or TiO_y. This peak is much suppressed or almost absent for mixed oxide layers of Ru + Ti as well as Ru + Ir and Ru + Pt, produced by thermal decomposition on a Ti substrate.

On the basis of the voltammetry curves, the RuO_x can be reduced and reoxidized over a substantial range of potentials in both acid and alkaline solution. The oxidation and reduction products appear to involve a single phase in view of having the voltammetry current density high over the wide potential range of the sweep rather than having the charge associated with a single voltammetry peak, even at very low sweep rates. The total charge associated with the area under the voltammetry curves in the cathodic or anodic sweeps between 0.1 and 1.4V is approximately 0.1 C/cm^2 of apparent area for the electrodes with 1×10^{-5} moles Ru/cm^2, or approximately one-tenth of that required to change the valency state by one electron per Ru atom in the oxide coating.

Kozawa (11) has reported that porous bulk hydrated RuO_2 can be reduced rather reversibly over an extended voltage range when mixed with carbon in both alkaline and acid solutions. The initial open-circuit voltage observed by Kozawa starting with near stoichiometric RuO_2 was +0.5V and +0.8V vs. RHE for the anhydrous and hydrated materials, respectively. Even considering the question of the reversibility of these potential measurements, it appears likely that the O_2 evolution reaction on RuO_x on Ti occurs in a potential range where at least the surface Ru ions of the catalyst are in a higher valency state than +4.

A large cathodic peak was observed in the voltammetry curves for the RuO_x on Ti electrodes in N_2 saturated KOH solutions in the potential range 0.6 to 0.9V when the anodic limit of the sweep was extended beyond 1.4V (see Figure 6). Saturation of the solution with O_2 rather than N_2 increased this peak. The potential range corresponds to that expected for O_2 reduction to HO_2^-. The assignment of this peak to the reduction of O_2 to peroxide was confirmed by adding the H_2O_2 to the solution and observing complementary cathodic and anodic peaks (see Figure 7). Thus in alkaline solutions, O_2 reduction on RuO_x/Ti electrodes involves solution phase HO_2^- as an intermediate.

3. ESCA and x-ray diffraction measurements

An effort has been made to examine the relationship of catalytic activity to the crystal structure, surface structure and sample preparation temperatures. X-ray diffraction studies of this material indicate a rutile-type of structure similar to that of single crystal RuO_2. The x-ray results also indicate that the catalytically active material which is prepared at 450°C is not a well crystallized sample. The x-ray lines are displaced from those of RuO_2 as well as being much broader. As the temperature of the sample preparation is increased to 650°C the lines become narrower and shift towards those of well crystallized RuO_2 indicating either an increased ordering in the crystals or a growth in crystallite size. A further interesting result from the x-ray data for samples prepared at 650°C is a decrease in the intensity of the lines due to the titanium

metal substrate with a simultaneous increase in the intensity of the lines due to TiO_2.

ESCA has been used to determine the composition of the catalyst surface. The surface of the catalyst was found to contain ruthenium in the four valent state and oxygen in the form of bound water, hydroxyl and O^{2-}. Some residual chloride was also found. In the samples prepared at low temperatures (e.g., 450°C) there appear to be two forms of chloride while at the higher temperature only one form.

As the above changes occur, the catalytic activity falls off. Several explanations are possible including: 1) the catalytic activity may be critically dependent on surface defects and the concentration of such surface defects is greatly reduced upon recrystallization; 2) the growth of large crystals results in a large loss in surface area; and 3) the growth of a non-conducting TiO_2 layer between the metal substrate and the RuO_x layer may lead to ohmic losses and an apparent loss of catalytic activity.

4. Polarization measurements

Figure 8 indicates the log current density vs potential data obtained potentiostatically for a RuO_x/Ti electrode with a very slow sweep (1 mV/sec) in O_2 saturated 4M KOH at a rotation rate of 8800 rpm. The hysteresis evident in this type of plot is very pronounced at low current densities because of the small currents associated with intrinsic changes in the oxidation state of the catalyst even at such slow sweep rates.

The anodic branch for O_2 generation is free of hysteresis effects above 5×10^{-3} A/cm^2 (apparent area) and exhibits a Tafel slope of 0.040V/decade over 3 decades after IR drop correction. Measurements in KOH-K_2SO_4 solutions of varying pH with constant K^+ ion concentration indicate a reaction order of 1.0 with respect to OH^- for the O_2 generation reaction over the pH range 11 to 14 (see Figure 9). With the electrode stationary and control of the boundary layer by O_2 bubble evolution, an anodic limiting current density has been observed in the KOH-K_2SO_4 electrolytes, which is directly proportional to the OH^- ion concentration from pH 10 to 14, amounting to $\sim$0.02 A/cm^2 (apparent area) at pH 11.8. Above the limiting current density, the discharge is from water with a Tafel slope of $\sim$0.13V/decade, indicating a change in mechanism.

Unfortunately the stoichiometric number cannot be obtained for the O_2 generation reaction in the alkaline solutions because of the interference from the intrinsic electrochemistry of the RuO_x/Ti electrode surface at low current densities near the reversible potential for the 4-electron reaction.

The Tafel slopes are independent of the catalyst loading over the ranges 10^{-8} to 10^{-5} moles Ru/cm^2 and the apparent exchange current densities are approximately proportional to the catalyst loading over this range (see Figure 10). Such a proportion is to be expected since the true-to-apparent area ratio is also approximately proportional to the catalyst loading.

The current density passes through zero in the anodic sweep

and increases very substantially cathodically during the cathodic sweep at approximately 0.90V as a consequence of the O_2 - HO_2^- reaction. The dependence of the O_2 reduction current density on rotation rate (f) at constant potential indicates that the O_2 reduction is under combined diffusion and kinetic control (see Figure 11).

The rotating disk data can be explained (4) on the basis of the following two reduction processes:

Reaction 1: $$O_2 + H_2O + 2e^- \xrightarrow{\vec{k}_1} HO_2^- + HO^- \quad (5)$$

Reaction 2: $$HO_2^- + H_2O + 2e^- \xrightarrow{\vec{k}_2} 3HO^- \quad (6)$$

The possibility can not be ruled out that some of the O_2 may also be reduced by a direct 4 electron reduction process:

Reaction 3: $$O_2 + 2H_2O + 4e \xrightarrow{k_3} 3HO^- \quad (7)$$

proceeding in parallel with reactions 1 and 2. Further measurements with the rotating ring-disk technique are needed to check this point.

V. DISCUSSION OF O_2 REDUCTION AND GENERATION KINETICS ON RuO_x/Ti

Since the cathodic and anodic branches for the oxygen electrochemistry on RuO_x/Ti in alkaline solutions are distinctly different, the results for each will be discussed separately.

A. Cathodic Branch

The parallel and series reaction schemes represented by equations 5 - 7 can be considered as part of the overall scheme shown in Figure 12 for alkaline solutions. The difference

between the series and parallel mechanisms then is just a matter of the reversibility of the adsorption-desorption of HO_2^- (step C). If this step is very irreversible, then the parallel scheme is the more appropriate representation.

The $4e^-$ overall reduction of O_2 may also proceed by a parallel reaction which does not involve a peroxide species on the surface. In view of the strength of the O-O interaction in O_2, this seems rather unlikely.

The assumption has been made in Figure 12 that the O_2 must be first adsorbed on the electrode prior to the first electron step but the adsorption may be electrochemical; i.e., simultaneous adsorption-electron transfer:

$$O_2 + e^- \longrightarrow O_2^-(ads) \qquad (8)$$

or

$$O_2 + HOH + e^- \longrightarrow HO_2(ads) + HO^- \qquad (9)$$

A separate O_2 adsorption step, preceding the first electron transfer step, however, provides a convenient potential insensitive step to explain the small dependence of the intercept 1/i on potential in Figure 11. The possible reduction of O_2 and HO_2^- without adsorption at a position equivalent to the outer Helmholtz plane has not been included in Figure 12 on the basis that strong interaction is required with the electrode surface for the electron transfers to proceed at a reasonable rate.

B. Anodic Branch

Several of the reaction paths for O_2 generation tabulated by Damjanovic (12) for acid solutions can have Tafel slopes corresponding to dV/d ln i = 2RT/3F or 0.040V/decade when

modified to a form suitable for alkaline solutions. All have the common feature that the rate controlling step is a second electron rather than first electron transfer. With judicious choice of H_2O vs. OH^- as the reactant in the first and second electron transfer steps or proceeding proton transfer steps, it is possible to have the kinetics also first order in OH^-.

With electrode surfaces involving species with ionic character, the authors prefer to write the mechanism in such a way as to indicate the possibility of changes in the effective valency state of the catalyst sites. A simple mechanism compatible with the observed Tafel slope and reaction order is as follows:

$$\underline{\text{Step a}}: \quad S^z + OH^- \underset{k_{-a}}{\overset{k_a}{\rightleftharpoons}} (SOH)^z + e^- \text{ (fast)} \tag{10}$$

$$\underline{\text{Step b}}: \quad (SOH)^z \xrightarrow{k_b} (SOH)^{z+1} + e^- \text{ (slow)} \tag{11}$$

followed by subsequent processes yeilding finally O_2 and regenerating the site S^{+z}; for example,

$$\underline{\text{Step c}}: \quad \begin{matrix}(SOH)^{z+1} \\ (SOH)^{z+1}\end{matrix} + \begin{matrix}OH^- \\ OH^-\end{matrix} \longrightarrow \begin{matrix}S\text{—}O\text{-}H\text{--}OH^- \\ S\text{—}O\text{-}H\text{--}OH^-\end{matrix} \longrightarrow \begin{matrix}S^z \\ S^z\end{matrix} + \begin{matrix}O \\ O\end{matrix} + \begin{matrix}HOH \\ HOH\end{matrix} \tag{12}$$

The sites are probably Ru^{4+} but also could be higher valency state Ru ions or Ti ions. There sites are undoubtedly hydrated although the waters of hydration are not shown in the mechanism. With the Step b rate controlling, negligible back reactions and the coverage of $(SOH)^z$ and $(SOH)^{z+1}$ low, the current density is

$$i = 4F \cdot \frac{k_a k_b}{k_{-a}} C_{OH^-} \cdot \exp \frac{(1+\beta_2)FE}{RT} \tag{13}$$

where E is the electrode potential against an arbitrary pH insensitive reference electrode; k_a, k_{-a}, and k_b are the rate constants for Steps a and b at E = 0; and β_2 is the transfer coefficient for Step b. For the usual value of $\beta_2 = 1/2$, the Tafel slope then is (2RT/3F) (2.30) or 0.040V/decade with i first order in C_{OH^-}. If Step b is followed by the reaction indicated by Step c, then the stoichiometric number should be 2. Unfortunately the stoichiometric number is not known experimentally.

In Step a, the site S is a Ru ion of the oxide lattice. Step a involves the oxidation of the Ru to a higher valency state with partial transfer of electron charge from the OH species to Ru forming a $(RuOH)^z$ complex. Such a process should require much less energy than the formation of an OH free radical or a rather weakly adsorbed OH radical. Step b involves the further oxidation to $(RuOH)^{z+1}$, possibly followed by the formation of $(RuO)^z$ before proceeding with Step c. The RuO_x/Ti electrode surface may have some of the same features as the $Ru(NH_3)_5ORu\text{-}(NH_3)_4ORu(NH_3)_5^{7+}$ ion, reported by Earley and Razavi (13, 14) to oxidize OH^- homogeneously to form O_2. These species have the structure Ru-O-Ru-O-Ru^{7+}. Earley and Razavi have pointed out that Ru has a tendency to form species of coordination number 7 and that there are low lying antibonding π^* orbitals which can accept electron charge from OH^-. Thus the $(RuOH)^z$ intermediate (other species in the inner coordination sphere not shown) seems reasonable.

ACKNOWLEDGMENTS: The authors are pleased to acknowledge the support of this work by NASA-Ames and ONR.

REFERENCES:

1. Bockris, J. O'M., in Proc. Cornell International Symposium and Workshop on the Hydrogen Economy, Linke, S. ed., Cornell University, Ithaca, N. Y. 1975.

2. Miles, M., Kessel, G., Lee, P., Srinivasan, S., J. Electrochemical Soc. 123 332 (1976).

3. See e.g., MacDonald, J. and Conway, B. E., Proc. Royal Soc., 269, 419 (1962); Schultze, J. W. and Vetter, K. J., Electrochim. Acta, 18, 889 (1973); Damjanovic, A. and Jovanovic, B., J. Electrochem. Soc., 123, 374 (1976)

4. O'Grady, W., Iwakura, C., Huang, J. and Yeager, E., in Proc. Symposium on Electrocatalysis, Breiter, M. ed., The Electrochemical Society, Princeton, N.J., 1974, 286-302.

5. See e.g., South African Pat. 68/7371, 68/7482 (1968); German Pat. 2021422(1969); 2014746, 1915951(1970); British Pat. 1206863(1970).

6. Morcos, I. and Yeager, E., Electrochim. Acta, 15, 953 (1970).

7. Zurilla, R. and Yeager, E., "Oxygen Electrode Kinetics on Gold," ONR. Tech. Rept. 23, Case Western Reserve University, Cleveland, 1969.

8. Kozawa, A., J. Inorg. Nucl. Chem., 21, 315 (1961)

9. Kozawa, C., O'Grady, W.E., and Yeager, E., unpublished research.

10. Kuhn, A. and Mortimer, C., J. Electrochem. Soc., 120, 231 (1973).

11. Kozawa, A., "Electrochemical Reduction of RuO_2," Abstract No. 29, National Meeting Electrochemical Soc., Boston, Oct. 1973.

12. Damjanovic, A. in Modern Aspects of Electrochemistry, Vol. 5, Bockris, J. O'M. and Conway, B. E. eds., Plenum Press, N. Y., 1969, 369-483.

13. Earley, J. and Razavi, H., Inorg. Nucl. Chem. Letters, 9, 331 (1973).

14. Earley, J. and Fealey, T., Inorg. Chem., 12 323 (1973).

LIST OF FIGURES:

Figure 7 Effect of hydrogen peroxide on the cyclic voltammograms of Ru oxide on Ti electrode in 4M KOH (N_2 saturated). Sweep rate: 50mV/sec; temp.: ~22°C.

Figure 8 Current-potential data for RuO_x on Ti. Data obtained with sweep rate of 2mV/sec with rotating disk technique. Electrolyte: 4M KOH (O_2 saturated); catalyst loading; ~1 x 10^{-5} M Ru/cm^2 (apparent area); rotation rate: 8800 rpm; temp.: ~22°C. Solid curve: anodic current; dashed curve: cathodic current.

Figure 9 pH dependence of current density at 0.65V vs SHE. in KOH - K_2SO_4 solutions with K^+ = 1 M; temp.: ~22°C. Stationary electrode.

Figure 10 Exchange current densities for O_2 generation on catalyst loading for RuO_x/Ti electrodes; temp.: ~22°C; electrolyte 4 M KOH.

Figure 11 Dependence of current density on rotation rate for O_2 reduction on the RuO_x/Ti electrode. Electrolyte: 4 M KOH_2 (O_2-saturated); catalyst loading: 1 x 10^{-5} moles Ru/cm^2; temp. ~22°C. (Open and solid circles correspond to two different experiments).

Figure 12 Simplified representation of series and parallel mechanism involving peroxide.

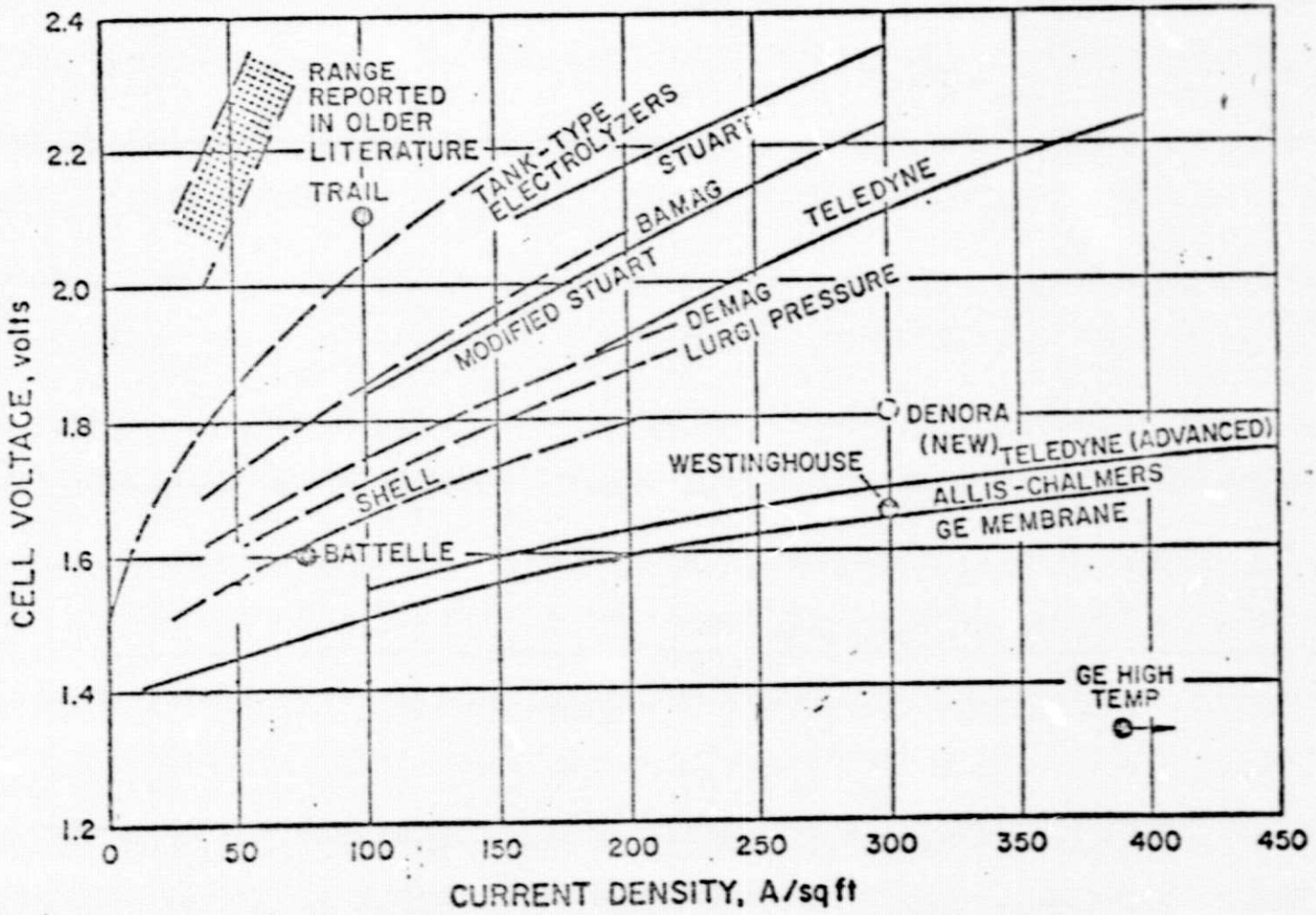

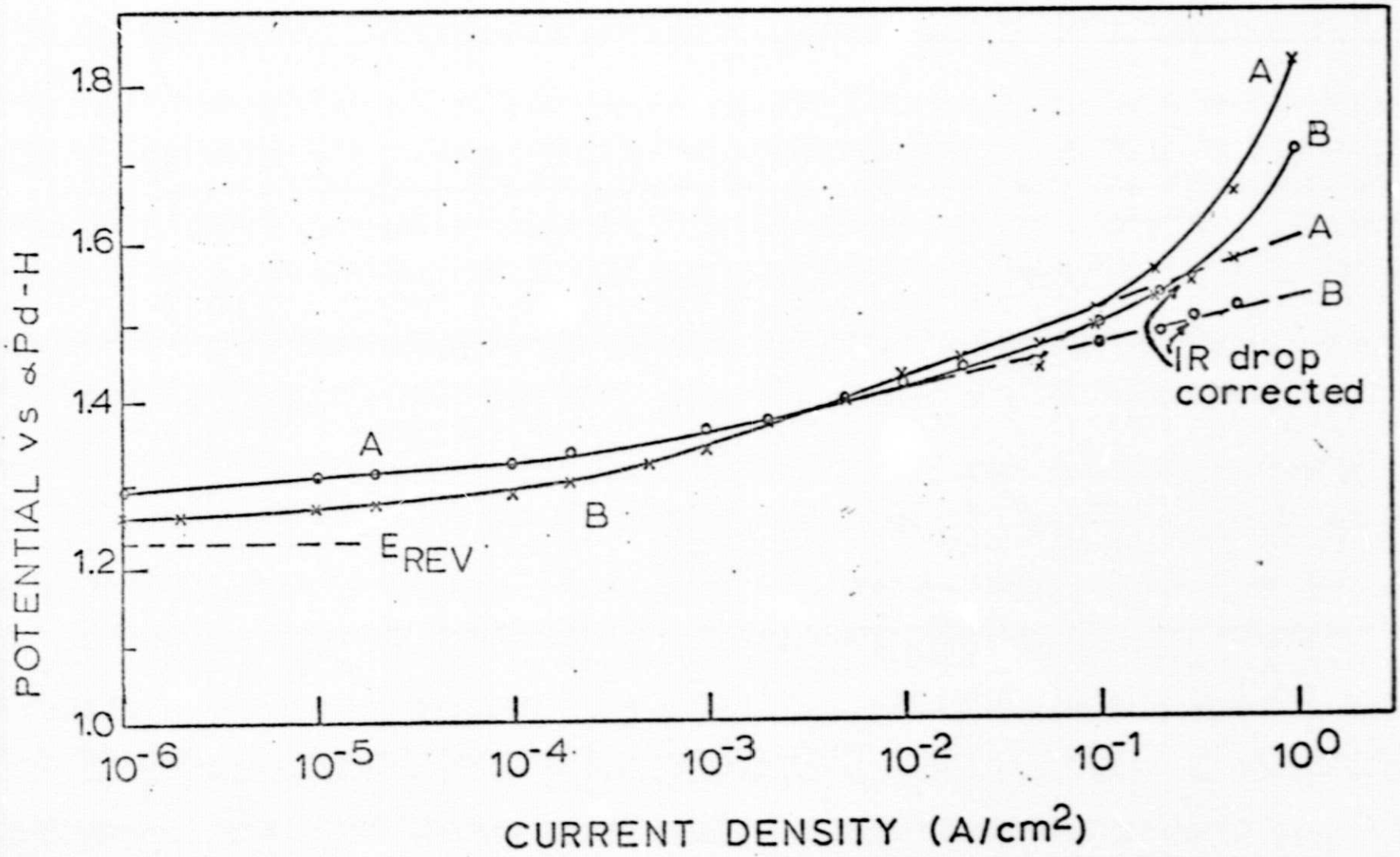
1.8
1.6
1.4
1.2
1.0
POTENTIAL vs αPd-H
A
B
A
B
A
B
IR drop
corrected
E REV
10-6
10-5
10-4
10-3
10-2
10-1
100
CURRENT DENSITY (A/cm2)

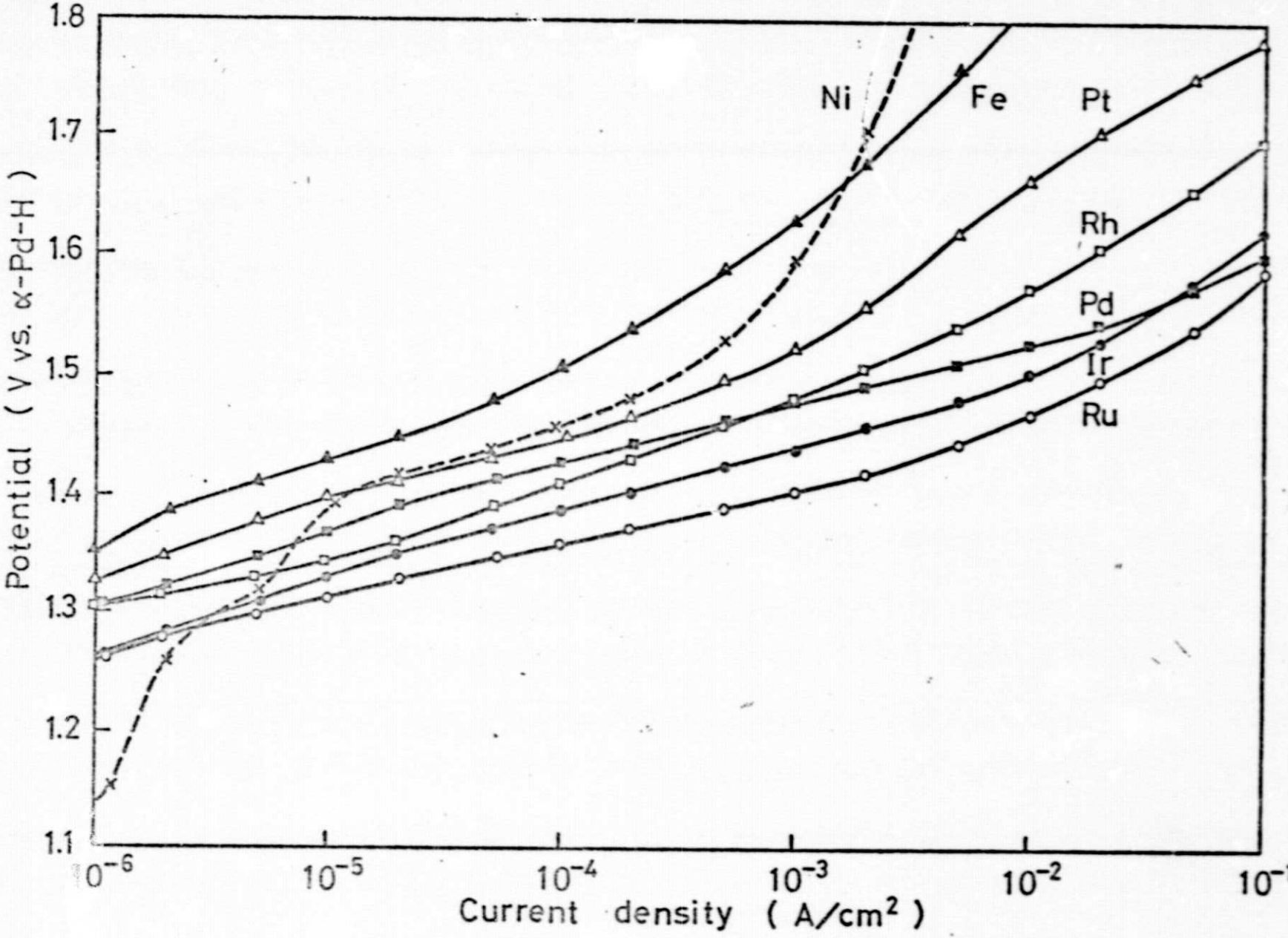
1.8
1.7
1.6
1.5
1.4
1.3
1.2
1.1
Potential (V vs. α-Pd-H)
Ni
Fe
Pt
Rh
Pd
Ir
Ru
10^{-6}
10^{-5}
10^{-4}
10^{-3}
10^{-2}
10^{-1}
Current density (A/cm^2)

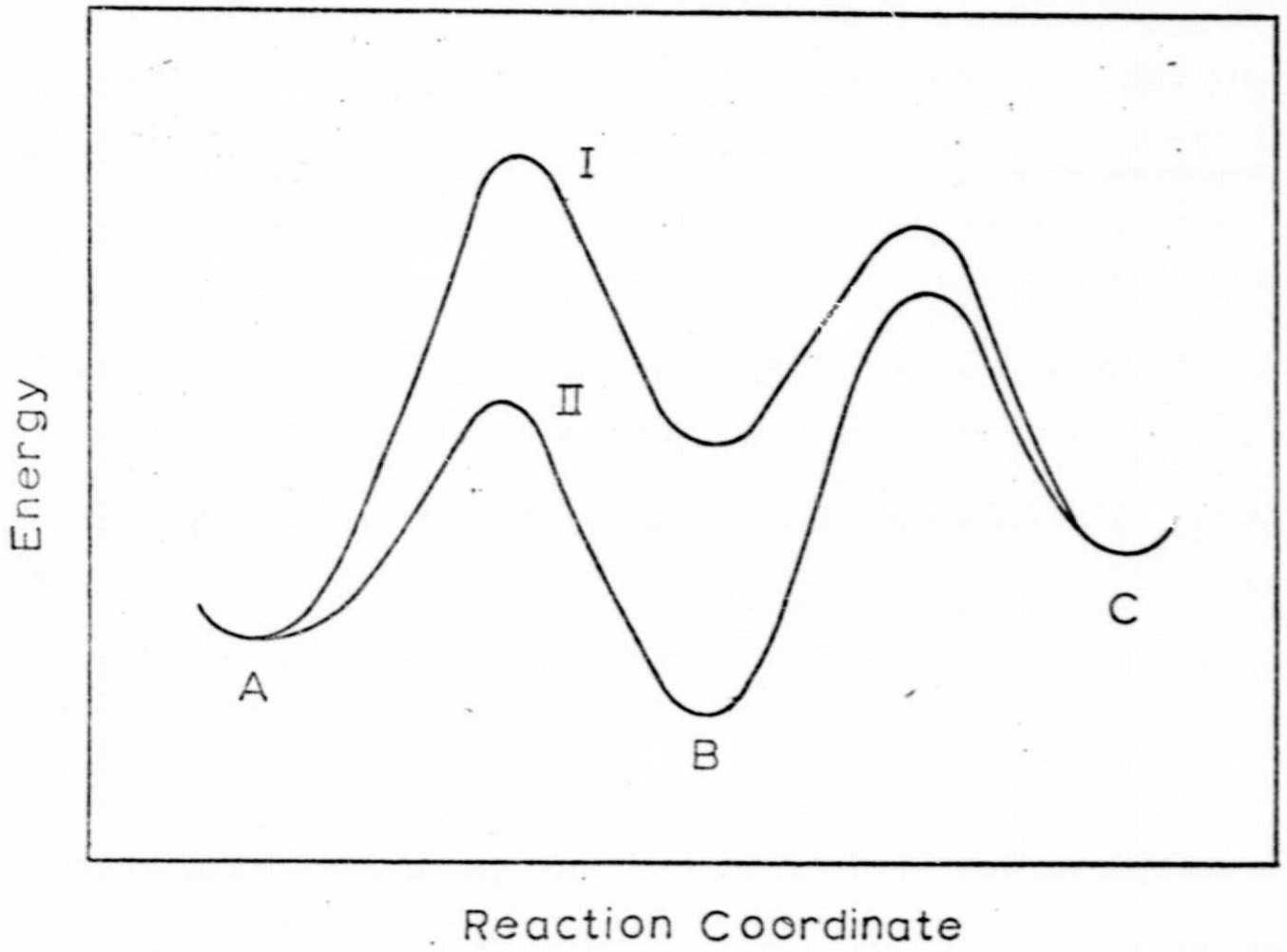
Energy
I
II
A
B
C
Reaction Coordinate

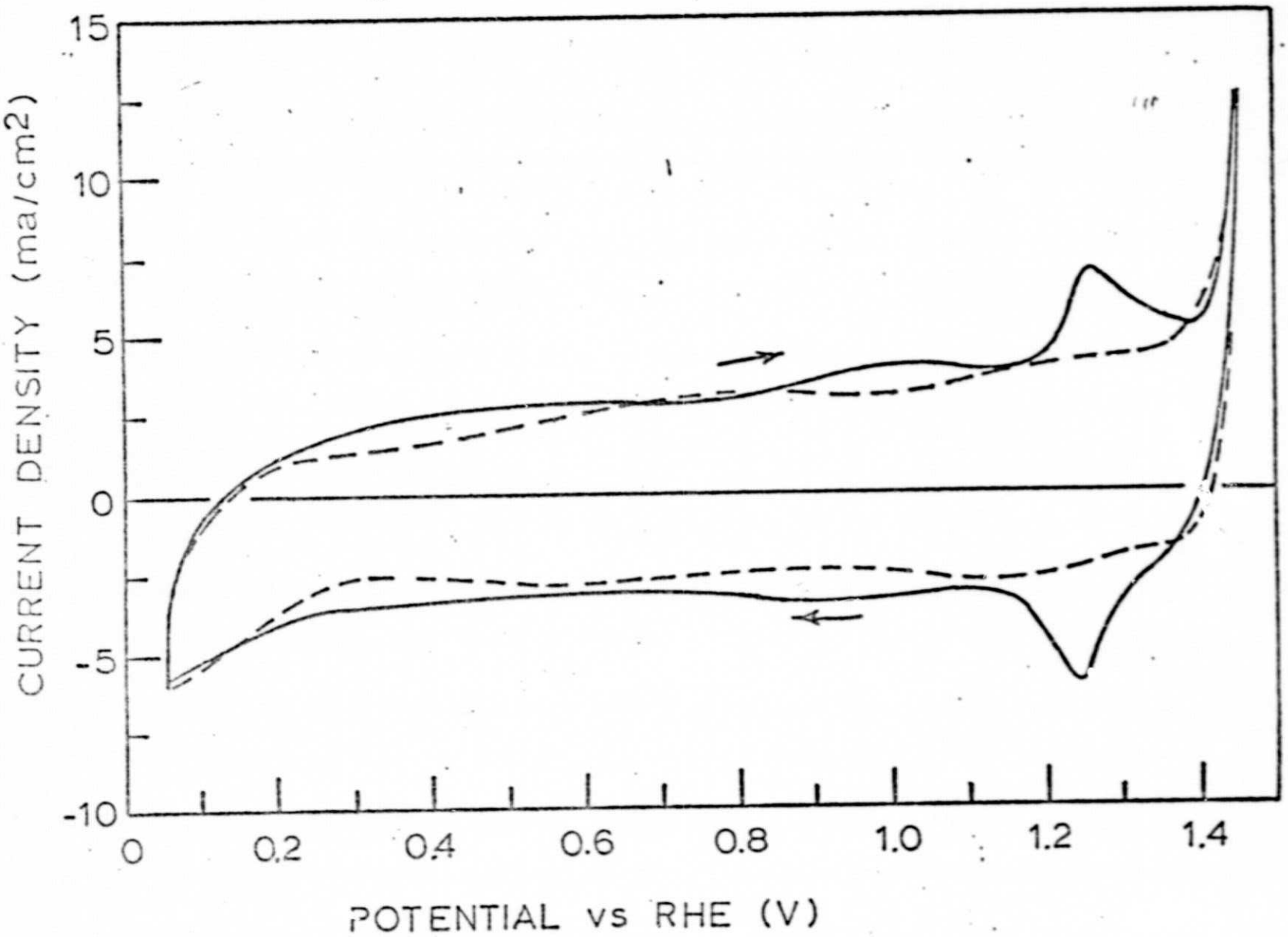
15
10
5
0
-5
-10
CURRENT DENSITY (ma/cm2)
0
0.2
0.4
0.6
0.8
1.0
1.2
1.4
POTENTIAL vs RHE (V)

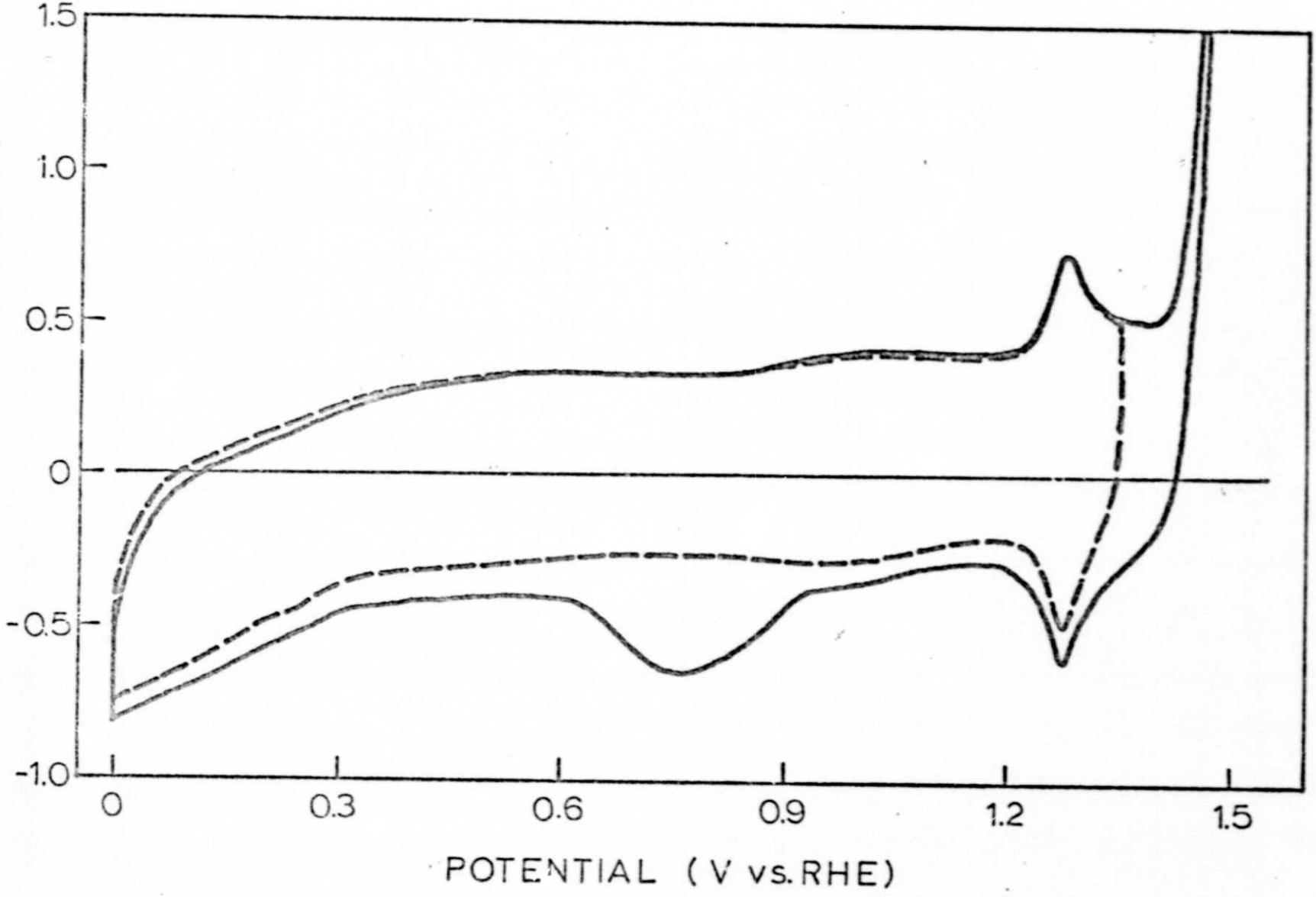

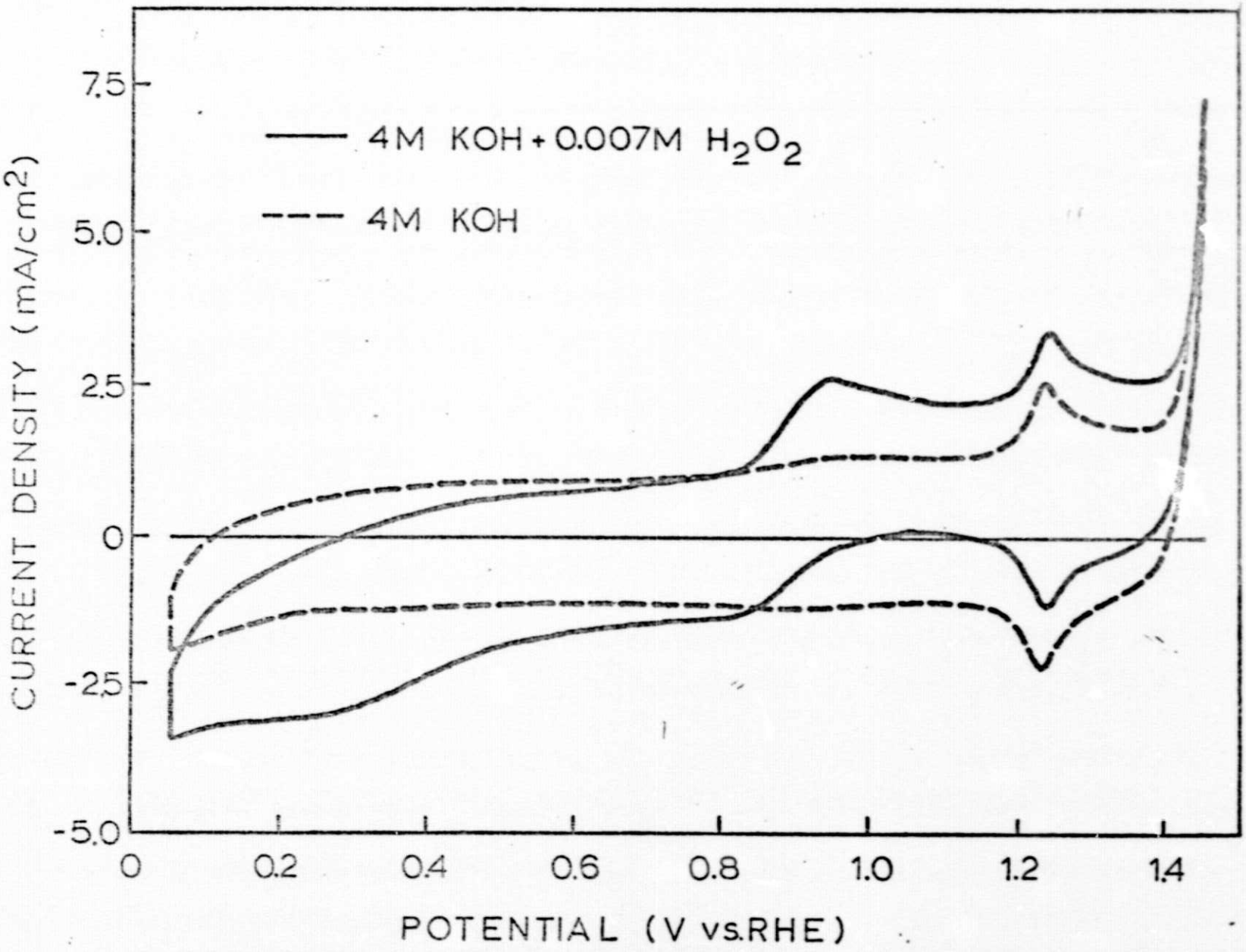
4M KOH + 0.007M H_2O_2
4M KOH
CURRENT DENSITY (mA/cm²)
7.5
5.0
2.5
0
-2.5
-5.0
0
0.2
0.4
0.6
0.8
1.0
1.2
1.4
POTENTIAL (V vs.RHE)

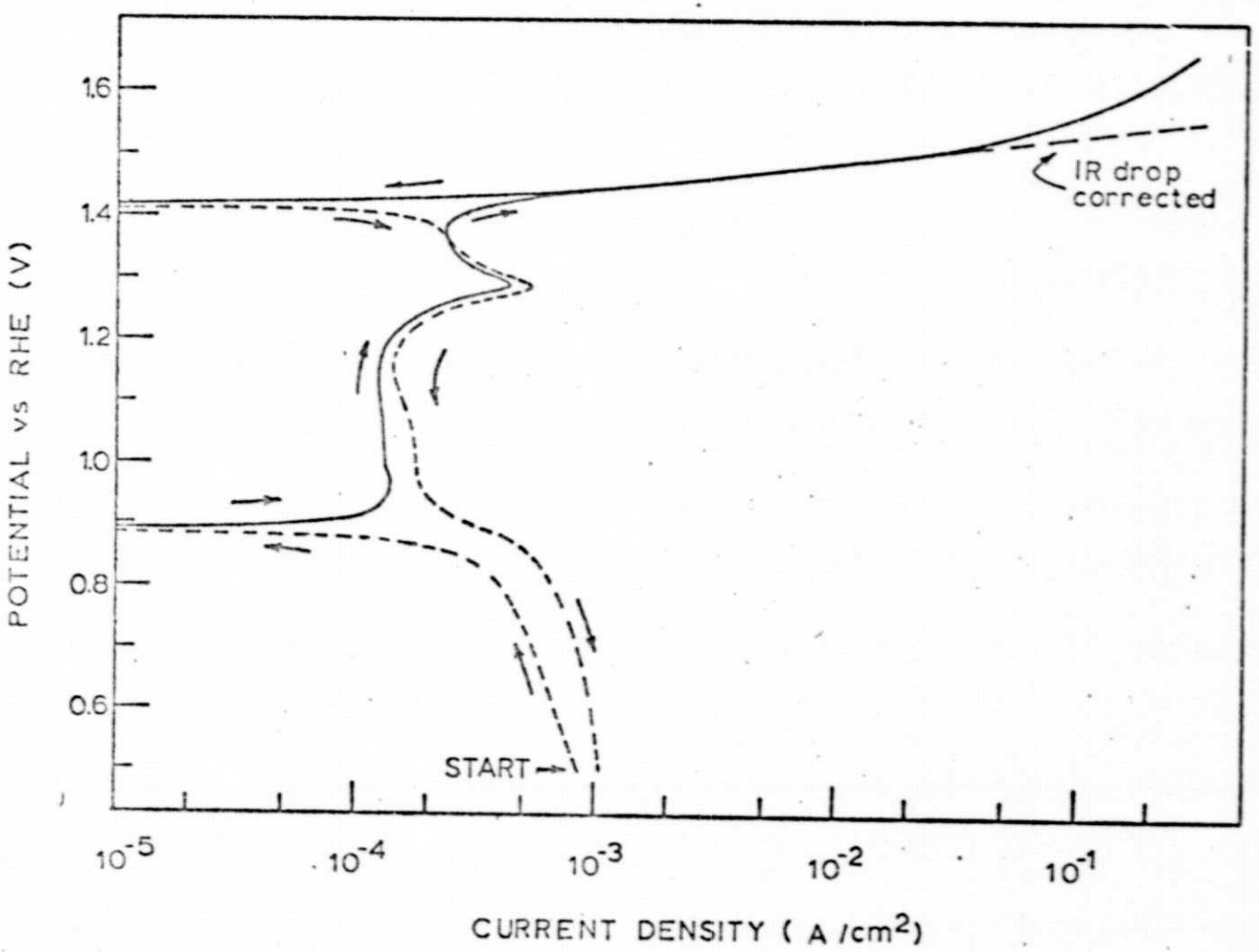
1.6
1.4
1.2
1.0
0.8
0.6
POTENTIAL vs RHE (V)
IR drop
corrected
START
10^{-5}
10^{-4}
10^{-3}
10^{-2}
10^{-1}
CURRENT DENSITY (A /cm^2)

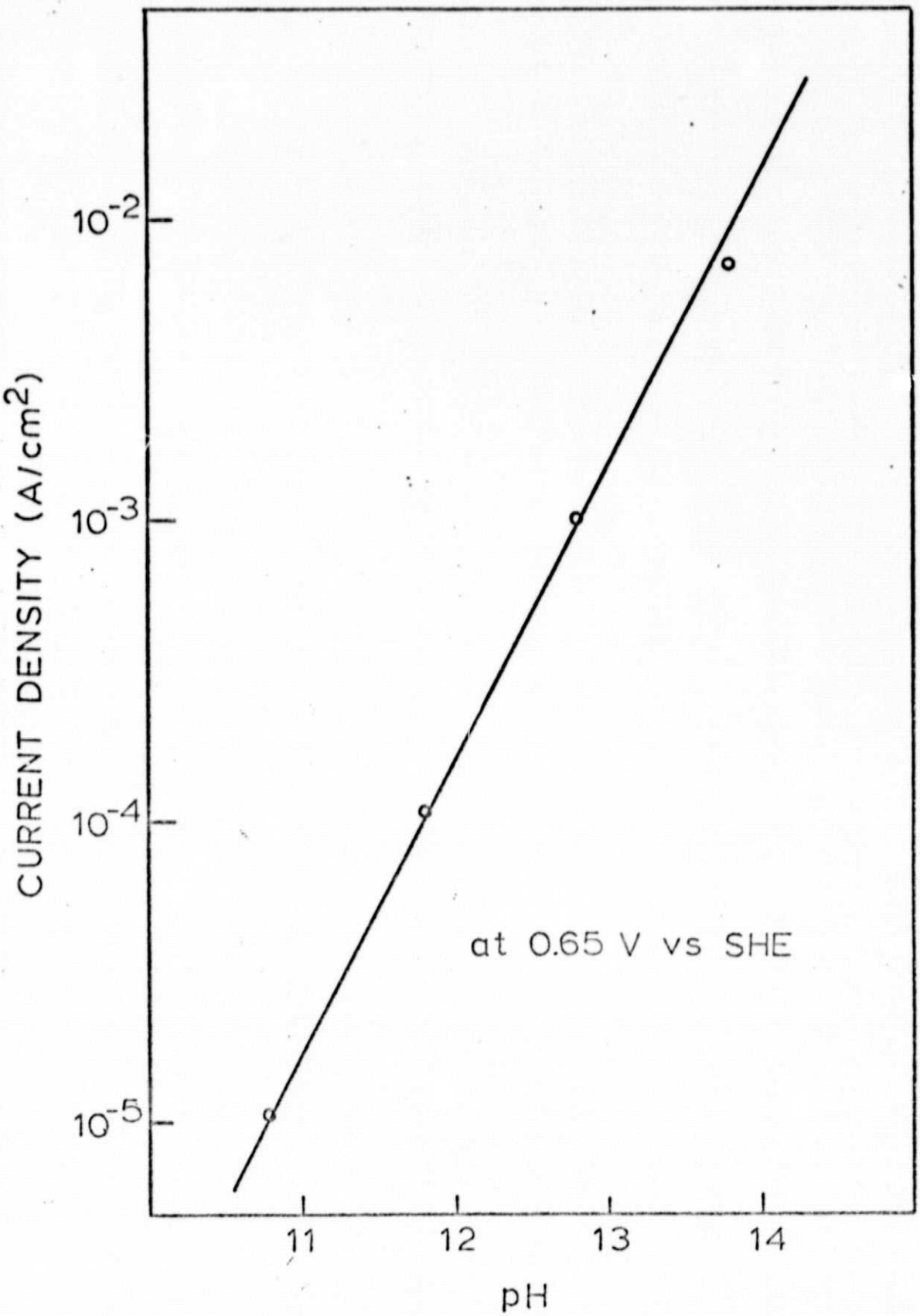
CURRENT DENSITY (A/cm²)
10⁻²
10⁻³
10⁻⁴
10⁻⁵
at 0.65 V vs SHE
11
12
13
14
pH

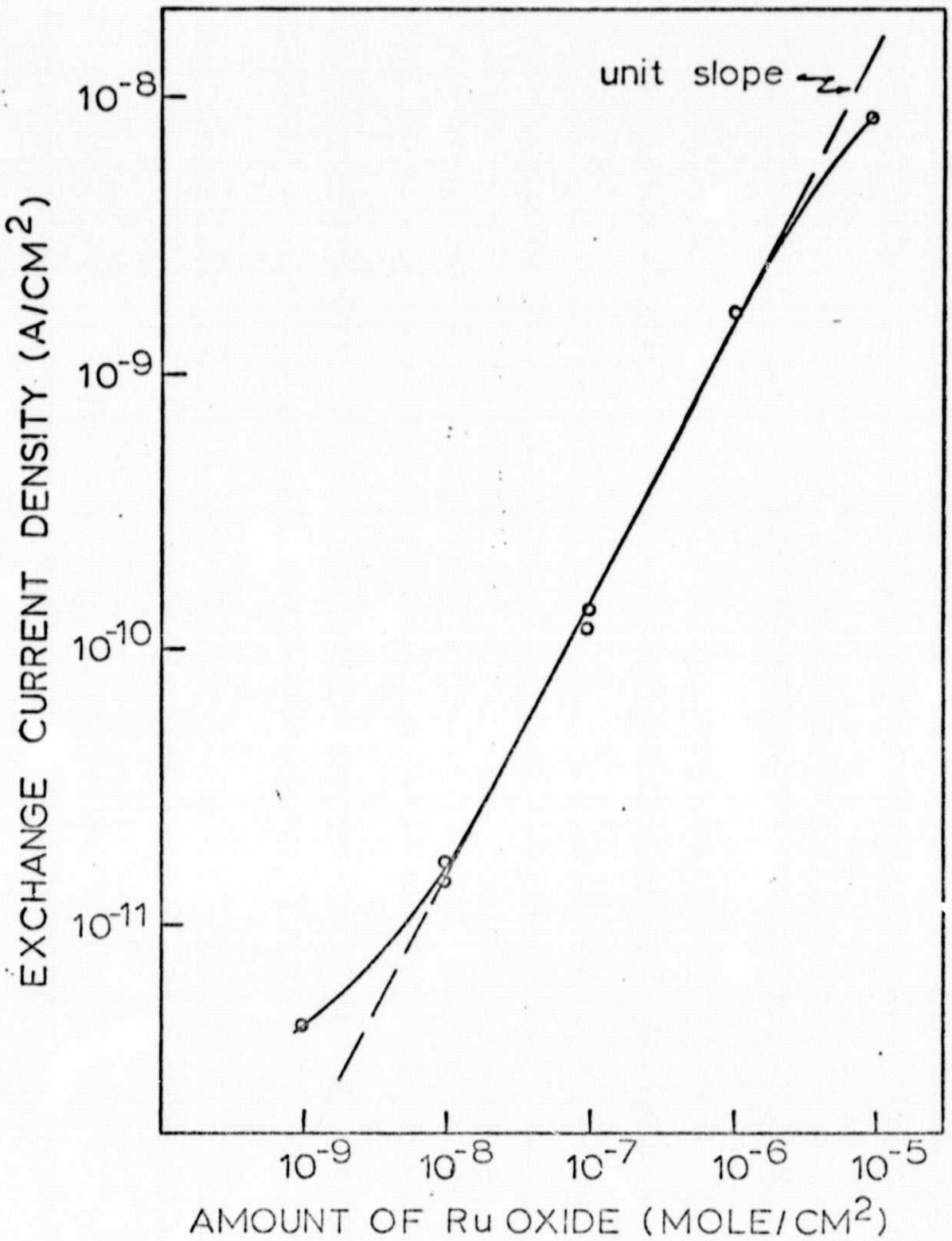
unit slope
EXCHANGE CURRENT DENSITY (A/CM^2)
10^{-8}
10^{-9}
10^{-10}
10^{-11}
10^{-9}
10^{-8}
10^{-7}
10^{-6}
10^{-5}
AMOUNT OF Ru OXIDE (MOLE/CM^2)

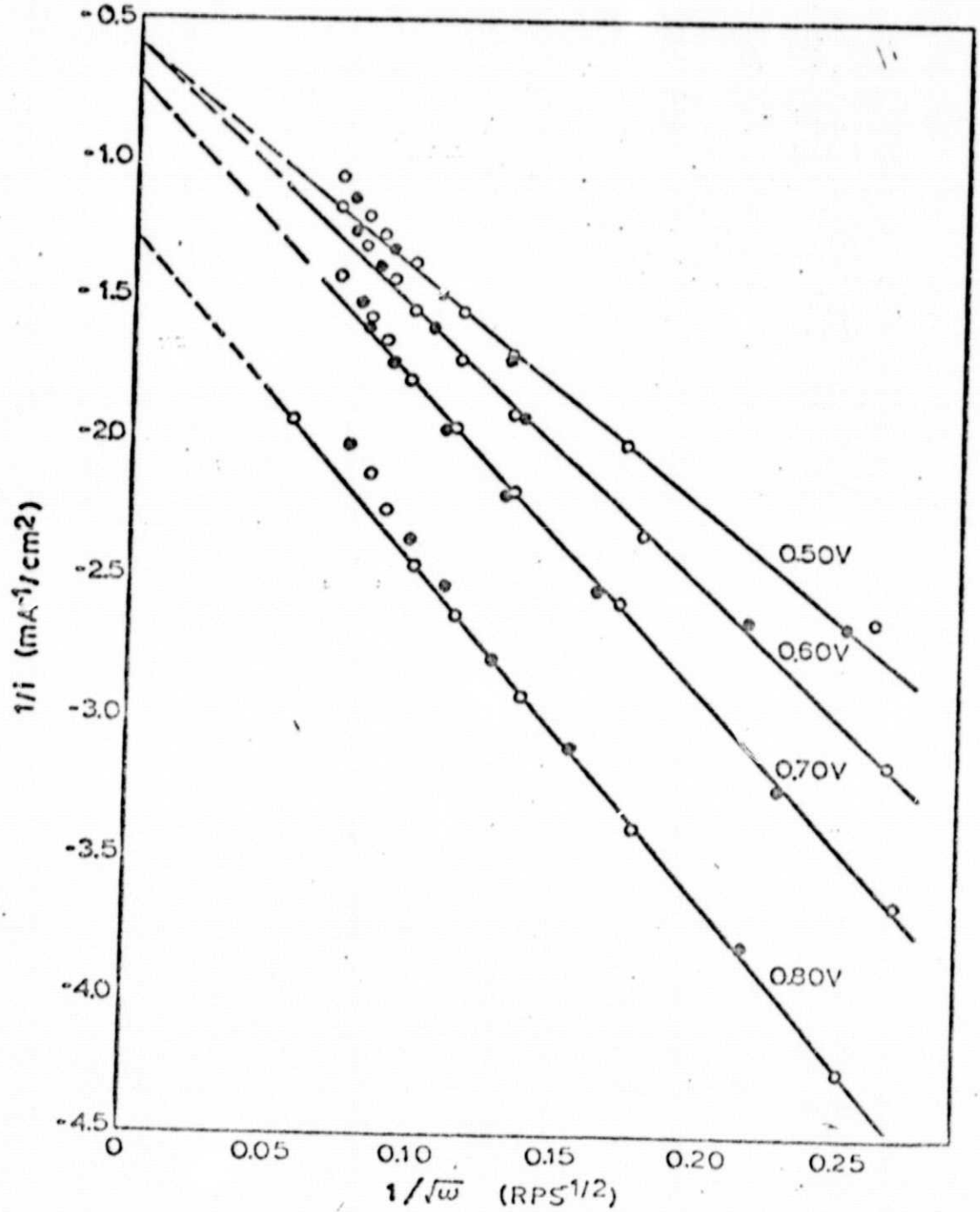
-0.5
-1.0
-1.5
-2.0
-2.5
-3.0
-3.5
-4.0
-4.5
1/i (mA⁻¹/cm²)
0
0.05
0.10
0.15
0.20
0.25
1/√ω (RPS^1/2)
0.50V
0.60V
0.70V
0.80V

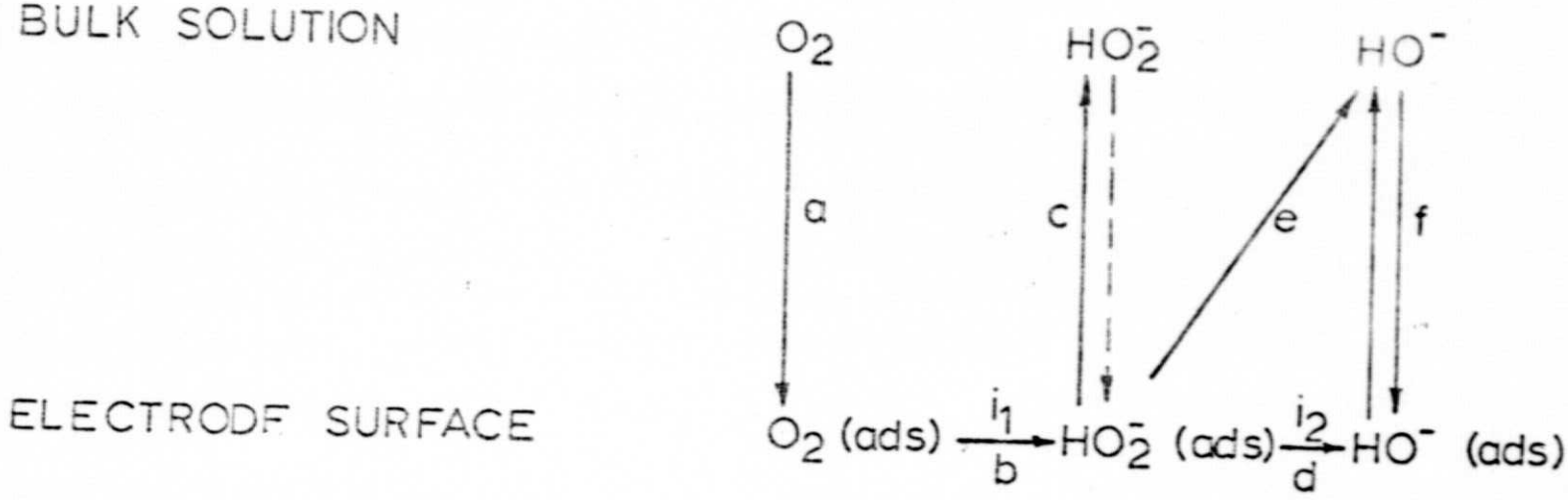
BULK SOLUTION
ELECTRODF SURFACE
O_2
HO_2^-
HO^-
a
c
e
f
O_2 (ads)
i_1
b
HO_2^- (ads)
i_2
d
HO^- (ads)